





A Case Study of Interstellar Material Delivery: α Centauri

Cole R. Gregg^{1,2}  and Paul A. Wiegert^{1,2} ¹ Department of Physics and Astronomy, The University of Western Ontario, London, Canada² Institute for Earth and Space Exploration (IESX), The University of Western Ontario, London, Canada

Received 2024 December 13; revised 2025 January 24; accepted 2025 January 31; published 2025 March 6

Abstract

Interstellar material has been discovered in our solar system, yet its origins and details of its transport are unknown. Here, we present α Centauri as a case study of the delivery of interstellar material to our solar system. α Centauri is a mature triple star system that likely harbors planets, and is moving toward us with the point of the closest approach approximately 28,000 yr in the future. Assuming a current ejection model for the system, we find that such material can reach our solar system and may currently be present here. The material that does reach us is mostly a product of low ($<2 \text{ km s}^{-1}$) ejection velocities, and the rate at which it enters our solar system is expected to peak around the time of α Centauri's closest approach. If α Centauri ejects material at a rate comparable to our own solar system, we estimate the current number of α Centauri particles larger than 100 m in diameter within our Oort Cloud to be 10^6 , and during α Centauri's closest approach, this will increase by an order of magnitude. However, the observable fraction of such objects remains low as there is only a probability of 10^{-6} that one of them is within 10 au of the Sun. A small number (~ 10) of meteors $>100 \mu\text{m}$ from α Centauri may currently be entering Earth's atmosphere every year: this number is very sensitive to the assumed ejected mass distribution, but the flux is expected to increase as α Centauri approaches.

Unified Astronomy Thesaurus concepts: [Interstellar objects \(52\)](#); [Meteor radiants \(1033\)](#); [Meteor streams \(1035\)](#)

Materials only available in the [online version of record](#): animations

1. Introduction

To date, there have been two discoveries of macroscopic objects from outside of our solar system: 1I/'Oumuamua (K. J. Meech et al. 2017) and 2I/Borisov (P. Guzik et al. 2020). At smaller sizes, in situ dust detectors on spacecraft (M. Baguhl et al. 1995; E. Grün et al. 1997; N. Altobelli et al. 2003) have also unambiguously detected interstellar particles. At intermediate sizes, the claims of interstellar meteors detected remain controversial. This is because usually the only indicator of the interstellar nature of a particle is its hyperbolic excess velocity, which is very sensitive to the measurement error (M. Hajdukova et al. 2020; M. Hajduková et al. 2024).

In any case, the details of the travel of interstellar material as well as its original sources remain unknown. Understanding the transfer of interstellar material carries significant implications as such material could seed the formation of planets in newly forming planetary systems (E. Grishin et al. 2019; A. Moro-Martín & C. Norman 2022), while serving as a medium for the exchange of chemical elements, organic molecules, and potentially life's precursors between star systems—panspermia (E. Grishin et al. 2019; F. C. Adams & K. J. Napier 2022; Z. N. Osmanov 2024; H. B. Smith & L. Sinapayen 2024).

Here, we aim to increase our understanding of interstellar transport by performing a case study of one particular nearby star system, α Centauri (α Cen), and focusing on transfer within the near term (last 100 Myr). The fundamental questions guiding this study are can α Cen plausibly be ejecting material at the current time, and if so, would we expect this material to arrive at our solar system? What would be the expected

characteristics of this material, including arrival direction, velocity, and flux?

The first question is whether α Cen can reasonably be expected to be ejecting material at the current time. As the system is mature, we would expect much of its original protoplanetary disk to have dissipated, with some of the mass possibly retained in asteroid/Kuiper belts, or an Oort cloud (OC). Our simulations examine the relatively recent past (astronomically speaking, ~ 100 Myr), well after any planet-forming phase and the disassociation of the birth cluster α Cen formed in (typical lifetimes are $\lesssim 100$ s Myr, F. C. Adams 2010). Therefore, the primary ejection mechanisms of interest are gravitational scattering of leftover planetesimals by the stars and/or planets within the system, as well as the loss of distant OC members to galactic tidal stripping. Much of the work along these lines was performed by S. Portegies Zwart (2021), who modeled the evolution of OCs around the 200 nearest Gaia stars for 1 Gyr in the past to determine the density of interstellar objects (ISOs) around the Sun, although α Cen is not discussed in detail in that work. Here, we seek to extract the specific details of the material delivery from that system near the present time, although we do not model the process of ejection in detail, but rather adopt a suitable ejection velocity distribution for the system.

Assuming that α Cen is currently ejecting material, we find that such material can reach our solar system and may currently be present here. This system is a good choice for this kind of case study for several reasons:

1. It is the closest star to our solar system, at 1.34 pc (R. Akeson et al. 2021). Its proximity increases the likelihood that material from this system can reach us.
2. It is approaching our solar system at 22 km s^{-1} (D. Evans 1967; P. Kervella et al. 2017; M. Wenger



Original content from this work may be used under the terms of the [Creative Commons Attribution 4.0 licence](#). Any further distribution of this work must maintain attribution to the author(s) and the title of the work, journal citation and DOI.

et al. 2000) and will pass within 200,000 au of the Sun in 28,000 yr. Thus, we can expect that the amount of material delivered to us is increasing as the effective cross section of the solar system increases (see Section 3 for more details).

3. This is a mature (5 Gyr age, F. Thévenin et al. 2002; M. Joyce & B. Chaboyer 2018; R. Akeson et al. 2021) triple star system that likely harbors planets. Although mature star systems likely eject less material than those in their planet-forming years, the presence of multiple stars and planets increases the likelihood of gravitational scattering of members from any remnant planetesimal reservoirs, much like how asteroids or comets are currently being ejected from our solar system.
4. Two of the stars, α Cen A and B, are Sun-like stars (see below for details). Their larger than typical stellar mass suggests that they likely formed from a more massive than typical protoplanetary disk, which might allow more mass to remain in an unaccumulated form. In particular, the system might have developed an OC, which results from gravitational scattering of planetesimals from Neptune mass planets (V. S. Safronov 1972; M. Duncan et al. 1987; S. Tremaine 1993), which would provide a source of macroscopic bodies to eject via mechanisms much like those seen in our solar system today (see Section 4.2).

Although we will not model the ejection process from α Cen in detail here, for dynamical context, we note that the system contains a $1.1 M_{\odot}$ and $0.9 M_{\odot}$ binary (α Cen A and B, respectively, spectral types G2V, K1, P. Morel et al. 2000), which has a highly eccentric orbit with a semimajor axis of 23.3 au and an orbital period of 80 yr (N. Cuello & M. Sucerquia 2024). The third star in the system, and the closest stellar neighbor to the Sun, is Proxima Centauri, a red dwarf orbiting the pair around 8200 au ($0.12 M_{\odot}$; M5.5V) (P. Kervella et al. 2017; I. Ribas et al. 2017). In 2016, G. Anglada-Escudé et al. (2016) reported the discovery of an Earth-sized planet in the habitable zone around Proxima. There have been other reports of planets in the Proxima system, including a possible sub-Earth-sized inner planet and a super-Earth or mini-Neptune (M. Damasso et al. 2020; R. Gratton et al. 2020; J. P. Faria et al. 2022). The binary system also has reported planetary candidates, but none confirmed (V. Rajpaul et al. 2015), although a planetary system is still believed possible (K. Wagner et al. 2021).

The triple star system orbits the Milky Way and is currently approaching the Sun, with an expected closest approach in $\sim 28,000$ yr. Thus, any material currently leaving that system at a low speed would be heading more-or-less toward the solar system. Broadly speaking, if material is ejected at speeds relative to its source that are much lower than its source system's galactic orbital speed, the material follows a galactic orbit much like that of its parent, but disperses along that path due to the effects of orbital shear (W. Dehnen & Hasanuddin 2018; S. Torres et al. 2019; S. Portegies Zwart 2021). This behavior is analogous to the formation of cometary meteoroid streams within our solar system, and which can produce meteor showers at the Earth.

Next, in Section 2, we outline the methods used for this study; in Section 3, we discuss the results; then, we turn to Discussion and Conclusions in Sections 4 and 5.

2. Methods

The study performs the numerical integration of particles released from α Cen over the last 100 Myr to examine the fastest dynamical pathways from that system to our solar system. The simulations are performed under the conditions described in the following sections.

2.1. Galactic Model

This work adopts a simple Galactic model for the Milky Way, which includes only the overall time-independent gravitational field. We neglect some known perturbations that affect small particles in particular, such as interstellar medium (ISM) drag and magnetic forces. As a result, our model is only applicable to particles above a certain size, which will be addressed in more detail later in this section and in the Discussion (Section 4.1).

Our simulations are conducted in a galactocentric reference frame, with the Galactic center (GC) positioned at the origin. A right-handed coordinate system has its x -axis extending through the Sun's projected position on the Galactic midplane toward the GC. The z -axis points toward the north Galactic pole. The y -axis is perpendicular to the x - z plane, with its positive direction determined by the right-hand rule.

The Galactic potential model we adopt is of M. Miyamoto & R. Nagai (1975), a three-component, time-independent, axisymmetric potential. The potential is smooth, and the force of gravity between individual stars is neglected. Individual star potentials can be neglected because the relaxation time, t_{relax} —the time for a body's orbit around the Galaxy to be significantly perturbed by interactions with individual stars—is known to be very long in the Milky Way, $t_{\text{relax}} \sim 10^7$ Gyr (J. Binney & S. Tremaine 2008), significantly longer than the age of the Galaxy, indicating that the effect can be neglected over the ~ 100 Myr timescales considered here.

The Galactic gravitational potential is represented by the sum of the three Galactic components:

$$\Phi = \Phi_b + \Phi_d + \Phi_h. \quad (1)$$

Provided in the galactocentric cartesian coordinate system

$$\Phi_{b,h} = -\frac{GM_{b,h}}{\sqrt{x^2 + y^2 + z^2 + b_{b,h}^2}}, \quad (2)$$

$$\Phi_d = -\frac{GM_d}{\sqrt{x^2 + y^2 + (a_d + \sqrt{z^2 + b_d^2})}}. \quad (3)$$

In these equations, G is the universal gravitational constant, M_i is the total mass of the Galactic component, and a_i , b_i are the scale lengths reflecting the geometries of the component. The bulge and halo are portrayed as spherically symmetric; therefore, only one scale length is required ($b_{b,h}$). The disk is represented as a flattened spheroid, which requires two scale lengths (a_d and b_d). The values we used to initialize our simulation are summarized in Table 1.

2.1.1. Particle Sizes

N. Murray et al. (2004) provide a detailed discussion of the influence of galactic magnetic fields, ISM drag, and grain destruction on interstellar particles, and all of these effects become increasingly important as the particle size decreases. The applicability of our model to smaller particles depends on the time and distance traveled in the ISM. We estimate that our

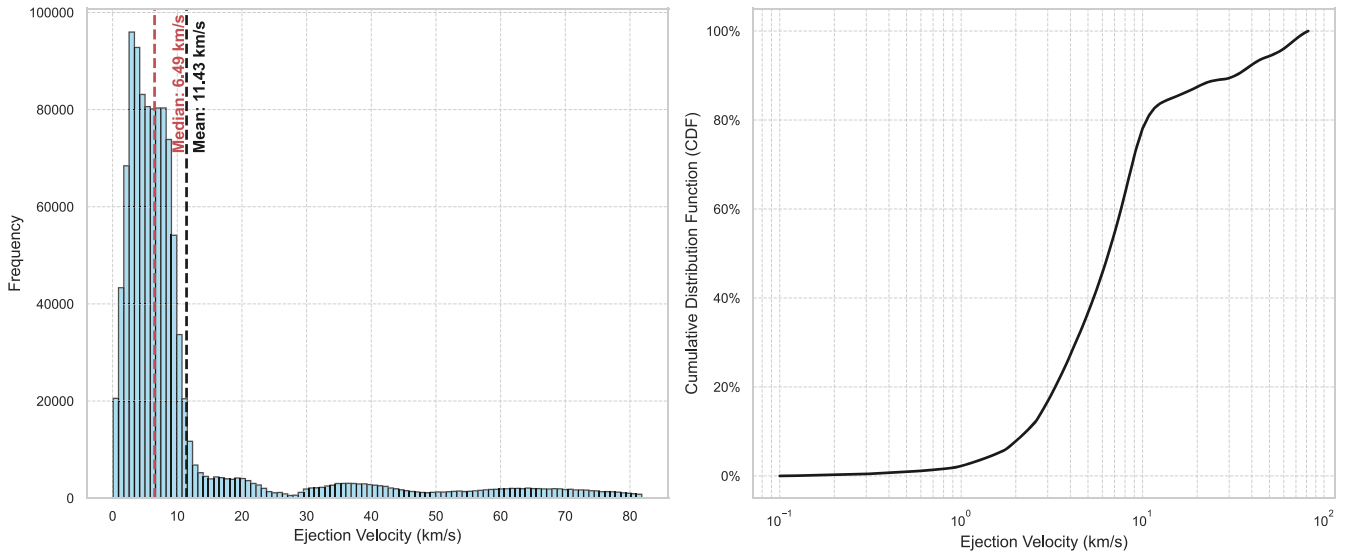


Figure 1. The ejection velocity distribution from our simulations, adapted from Figure 6 of C. A. L. Bailer-Jones et al. (2018; their red-dashed line). The right panel is our recreation of the C. A. L. Bailer-Jones et al. (2018) figure, showing the cumulative distribution of ejection velocities caused from a binary star system with masses $1 M_{\odot}$ and $0.1 M_{\odot}$ on a circular orbit of with 10 au separation.

Only a small fraction of the α Cen ejecta come within the CA distance of the Sun. In total, 350 particles had a CA with the solar system, $\sim 0.03\%$ of the total ejecta. The first CA arrives at $t \approx -2.85$ Myr. Material continues to arrive for ~ 10 Myr (Figure 3 and the corresponding animation) with the majority of CAs within $\pm 200,000$ yr of the current epoch (Figure 4). This peak is centered around α Cen’s time of closest approach to the solar system in $\sim 28,000$ yr. In that figure, we also include the effective cross section of the solar system (here, taken to be of 10^5 au radius) as viewed from α Cen and expressed as a solid angle. This cone reaches a maximum full-width of 37.5° when α Cen is at its point of closest approach, and we see that the rate of arrivals broadly coincides with and peaks at the same time. However, because the particle travel times are not zero, this is only an approximation of the effective cross section that they see, which depends on their relative velocity. Nevertheless, it illustrates that we expect material to be transferred more efficiently as our solar system’s apparent cross section grows as we move toward our point of the closest approach with α Cen.

The ejection speed distribution from a giant planet peaks between 1 and 2 km s^{-1} (C. A. L. Bailer-Jones et al. 2018); while in our simulations we find 52% of particles that arrive from α Cen have ejection speeds less than 2 km s^{-1} (with a maximum around 77 km s^{-1} , Figure 5). Thus, the speeds that most effectively move material from α Cen to us closely match those expected for an ejection by a massive planet, such as might occur due to the planets around Proxima Centauri, although no planets more massive than a mini-Neptune have been confirmed yet in the α Cen system.

The times of ejection (t_{eject}) that resulted in a CA ranged from $t_{\text{eject}} \approx -93$ Myr to $t_{\text{eject}} \approx -12,000$ yr. The majority of the CAs had ejection times closer to the current epoch ($\approx 53\%$ with $t_{\text{eject}} > -1$ Myr; $\approx 84\%$ with $t_{\text{eject}} > -10$ Myr), meaning that fresh ejecta was more likely to encounter the solar system (Figure 5). This is as expected, as the α Cen system is moving toward the Sun, and the solid angle the solar system subtends is largest when their mutual distance is smallest. The majority ($\approx 84\%$) of the CAs traveled for < 10 Myr, a fraction of a galactic orbit (Figure 6). These particles are therefore exposed

to the ISM for a relatively short time, lessening any effects from the galactic magnetic field, ISM drag, grain destruction, and perturbations from GMC encounters (discussed further in Section 4.1).

When the CAs intercept the solar system, their median apparent velocity relative to the Sun (Δv) observed at their closest approach is 32.50 km s^{-1} , ranging from 13.75 to 103.17 km s^{-1} (Figure 7). Due to the high fraction of CAs that resulted from low ejection speeds, we see the solar relative velocities center around the current apparent velocity of α Cen ($\Delta v = 32.37 \text{ km s}^{-1}$) as expected.

As particles fall into the solar system, their heliocentric speed v_{hel} increases beyond the relative speed Δv that they have at large distances. If they are observed on Earth as meteors, their observed heliocentric speed will be given by

$$v_{\text{hel}} = \sqrt{\Delta v^2 + \frac{2GM_{\odot}}{r_{\oplus}}} \quad (4)$$

where Δv is its velocity relative to the Sun when distant from our system, and r_{\oplus} is the Earth’s distance from the Sun. Using our minimum, median, and maximum values found, we can determine an expected range of heliocentric speeds in the inner solar system, at 1 au from Sun, to be $44 \lesssim v_{\text{hel}} \lesssim 111 \text{ km s}^{-1}$ with a median around 53 km s^{-1} .

3.1. Meteor Radiants

The heliocentric equatorial radiant of CAs is plotted in Figure 8, and also plotted and animated for the resulting “interstellar meteor shower” in Figure 9. The radiant would be the on-sky location from which the interstellar particle would appear to originate if it appeared as a meteor in Earth’s sky. The figure converts the solar relative velocity (Δv) to a heliocentric equatorial R.A. (α) and decl. (δ) for easy comparison with solar system meteor shower radiants. Two radiant clusters appeared in our simulations, one centered on an average position of $(\alpha, \delta) = (292^\circ \pm 1^\circ, -43^\circ \pm 2^\circ)$ and the other at $(\alpha, \delta) = (249^\circ \pm 17^\circ, -60^\circ \pm 8^\circ)$.

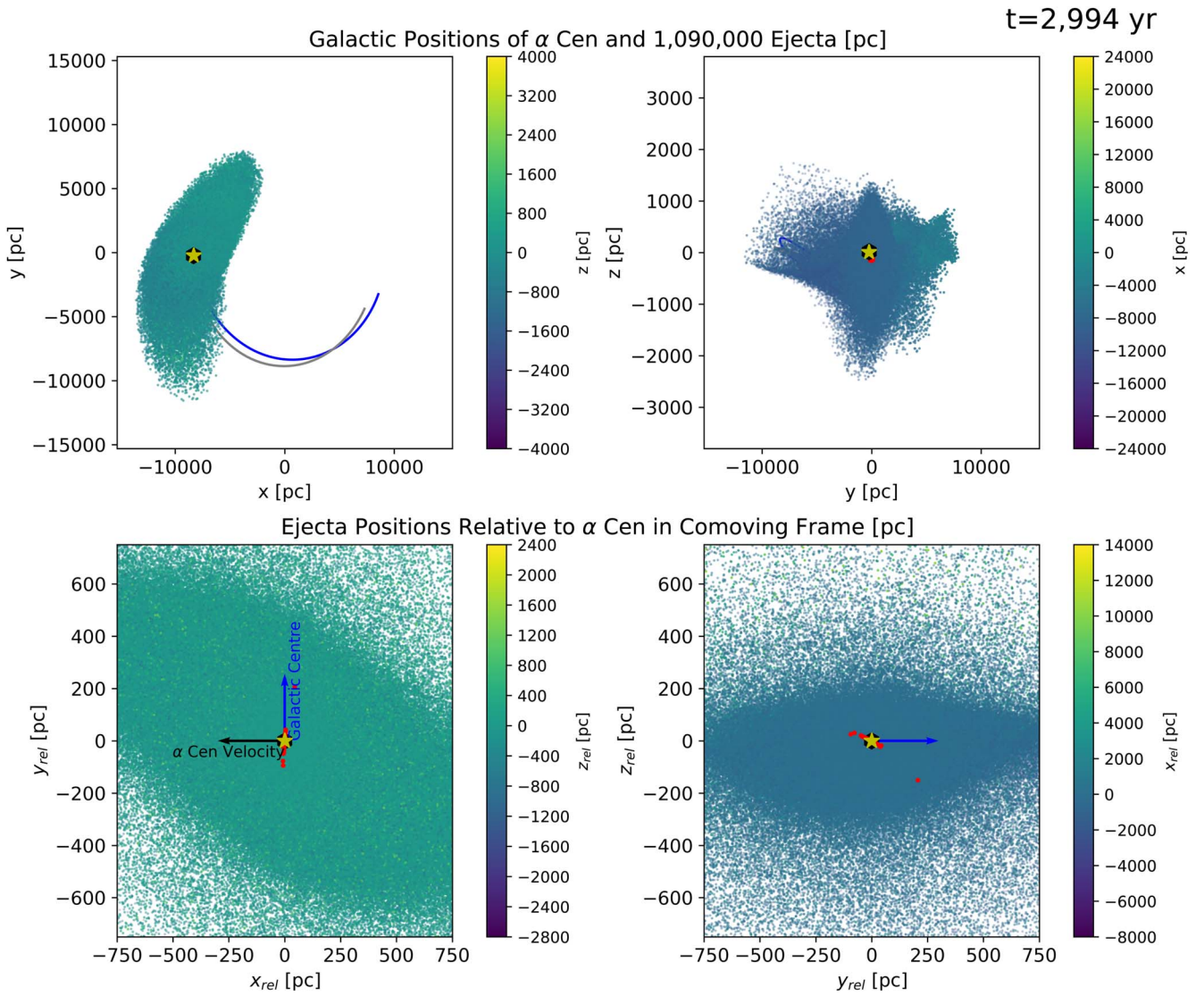


Figure 2. α Cen’s orbit about the Galactic center viewed on the x - y and y - z planes (top row), as well as the orbits of the ejecta from α Cen viewed in a comoving frame (bottom row). Our Sun (*Sol*) is marked by a black hexagon, and its orbital path indicated by a gray solid line (top row only). α Cen’s location and path are shown by a yellow star and blue solid line (top row only). In the bottom row, the comoving frame follows α Cen around its orbit while maintaining its orientation with the y -axis pointing toward the Galactic center (blue arrow) and α Cen’s velocity pointing in the x -direction (black arrow). This still frame is taken at $t \approx 3000$ yr (that is, +3000 yr from the current epoch) after ~ 100 Myr of integration. The colors of the ejecta represent the third dimension of position, except that any particle that will at any point come within 100,000 au of *Sol* are plotted in red. The full animation is available in the HTML version of this publication, which shows the time evolution from $t \approx -100$ Myr to $t \approx 10$ Myr. The duration of the animation is 11 s.

(An animation of this figure is available in the [online article](#).)

The first cluster is located at the on-sky position of what we term the “effective radiant,” the projection of the α Cen’s velocity vector relative to the Sun (reversed) onto the celestial sphere. Currently, α Cen’s motion relative to the Sun is one primarily of approach along the radial direction. Therefore, particles originating from it and that arrive here must be traveling along that nearly same line, and thus, the effective radiant coincides largely with α Cen’s position on the sky. One would expect the radiant of the stream to be in the approximate part of the sky as the origin star as it is approaching the solar system. In the animation linked to Figure 9, we do indeed see the majority of the CAs coming from the same direction as both the on-sky position of α Cen and its effective radiant, at least at times before the current epoch.

As α Cen passes its closest point to us, its motion changes from being mostly radial to mostly tangential. Although

particles continue to arrive in the solar system from the direction of the effective radiant, α Cen itself moves away from this point on the sky. The apparent cross section of our solar system is largest at the closest approach, allowing material ejected with a range of speeds within a much wider cone to reach us, creating the broad second radiant cluster.

After α Cen passes its closest approach, it begins to recede from us at 32 km s^{-1} ; however, low-speed material ejected in the past would still arrive from the same effective radiant. But at this point, it is difficult for material newly ejected from that system to reach us, and the rate of arrival of material from α Cen drops sharply.

The effective cross section of the solar system shows a smooth progression up to the peak intensity of the α Cen shower (Figure 4). In our simulation, we instead see a more sudden increase, which result from our discrete ejection

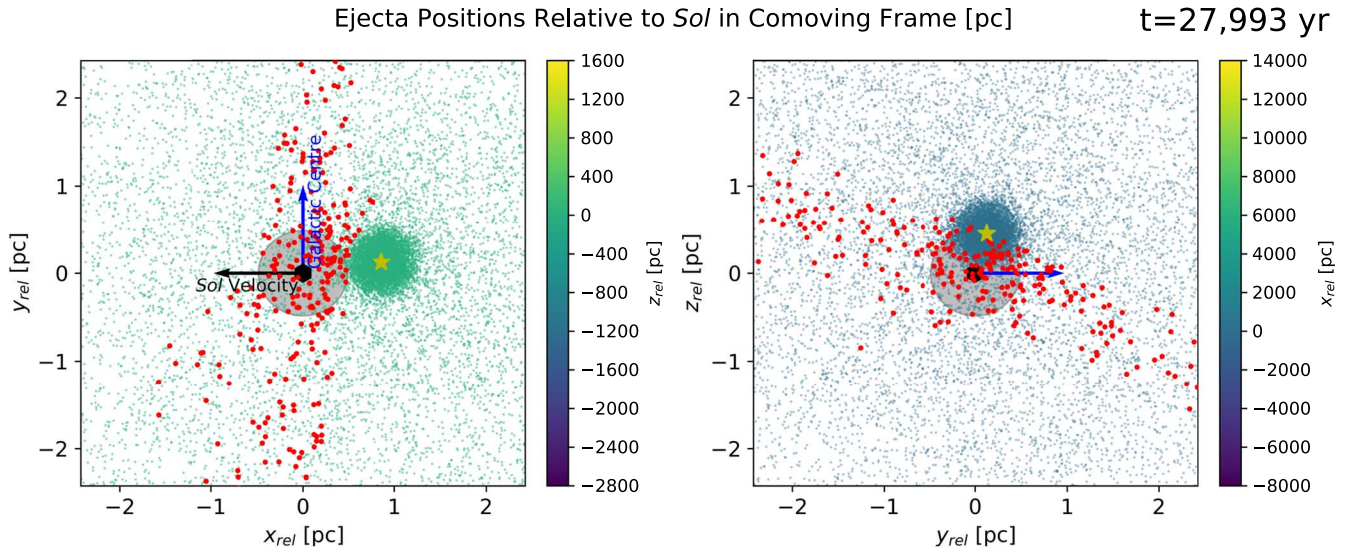


Figure 3. The paths of the ejecta from α Cen viewed in a comoving frame with *Sol*. The comoving frame follows *Sol* around its orbit maintaining the orientation with the y -axis pointing toward the Galactic center (blue arrow) and *Sol*'s velocity pointing in the x -direction (black arrow). Our Sun (*Sol*) is indicated by a black hexagon, and α Cen by a yellow star. This still frame is taken at closest approach to our solar system ($t \approx 28,000$ yr, years from the current epoch) after ~ 100 Myr of integration. The colors of the ejecta represent the third dimension of position. The gray circle represents the extent of the Oort cloud (100,000 au); any particle that comes within this distance of *Sol* at any point is flagged as a close approach. These particles are plotted in red. The full animation is available in the HTML version of this publication, which shows the shower duration from $t \approx -3$ Myr to $t \approx 7$ Myr. The duration of the animation is 44 s. (An animation of this figure is available in the [online article](#).)

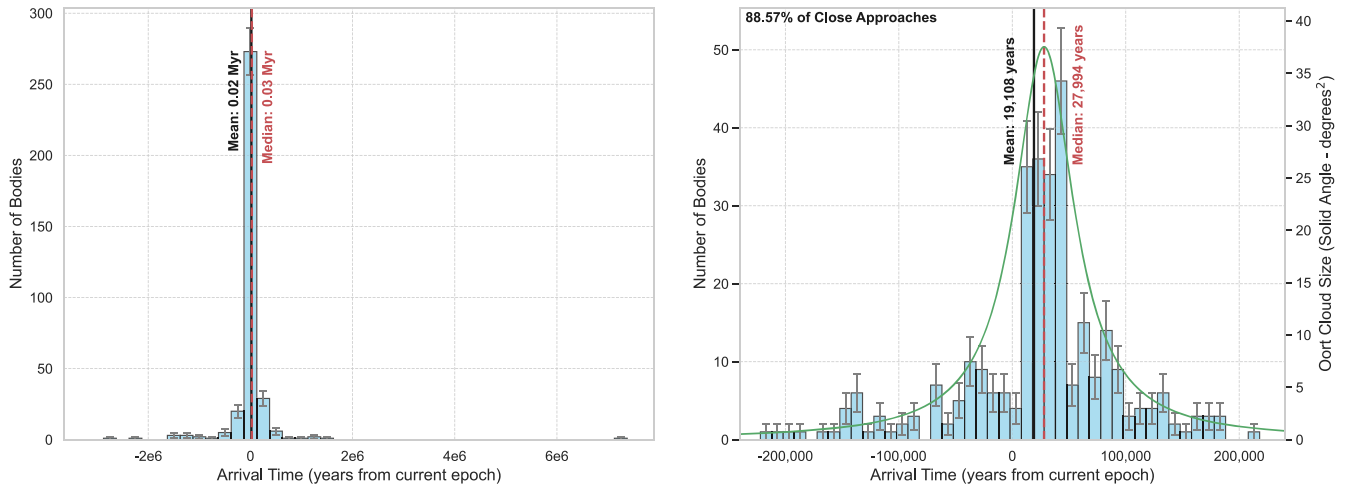


Figure 4. The arrival times at the solar system of the α Cen material. The left figure shows all close approaches while the right zooms into the time of peak intensity. The green line shows the effective cross section of the solar system (the solid angle subtended by our Oort cloud as seen from α Cen).

modeling. As we eject material every 1 Myr, we see a sudden burst of CAs around the time of α Cen's closest approach, and a sudden shift in the radiant, rather than a gradual change. To examine this in more details, we ran an auxiliary simulation just during the closest approach where the time between ejections was shortened. In this case, the CA radiants are smoothly dispersed along the path of the projected cross section of the solar system (purple shaded region in Figures 8 and 9) from a narrow cluster surrounding α Cen's effective radiant to the large region near α Cen's current on-sky position.

3.2. Are There α Cen Particles among Proposed Interstellars?

A selection of previously discovered/proposed interstellars is plotted alongside the observed radiants of our α Cen shower in Figure 9. Included are two confirmed macroscopic ISOs (1I/'Oumuamua and 2I/Borisov), traced back to their asymptotic

arrival directions (T. Hallatt & P. Wiegert 2020); five unconfirmed interstellar meteoroid candidates observed by the Canadian Meteor Orbit Radar (CMOR; M. Froncisz et al. 2020); three reported interstellar meteor influx directions detected by the Advanced Meteor Orbit Radar (W. J. Baggaley 2000; A. D. Taylor et al. 1996); along with confirmed interstellar dust (ISD) influx directions into the solar system as reported by spacecraft Cassini, Ulysses, and Galileo (V. J. Sterken et al. 2012). Other directions are also included for comparison, including the solar apex with respect to the local standard of rest (C. Jäschek & A. Valbousquet 1992); the solar apex with respect to the GC (solar galactic apex; M. J. Reid & A. Brunthaler 2004).

The list of values plotted in Figure 9 is provided in Table 2. None of these appears to be correlated with the directions expected for α Cen. Further analysis of meteor databases to search for α Cen-related events is encouraged.

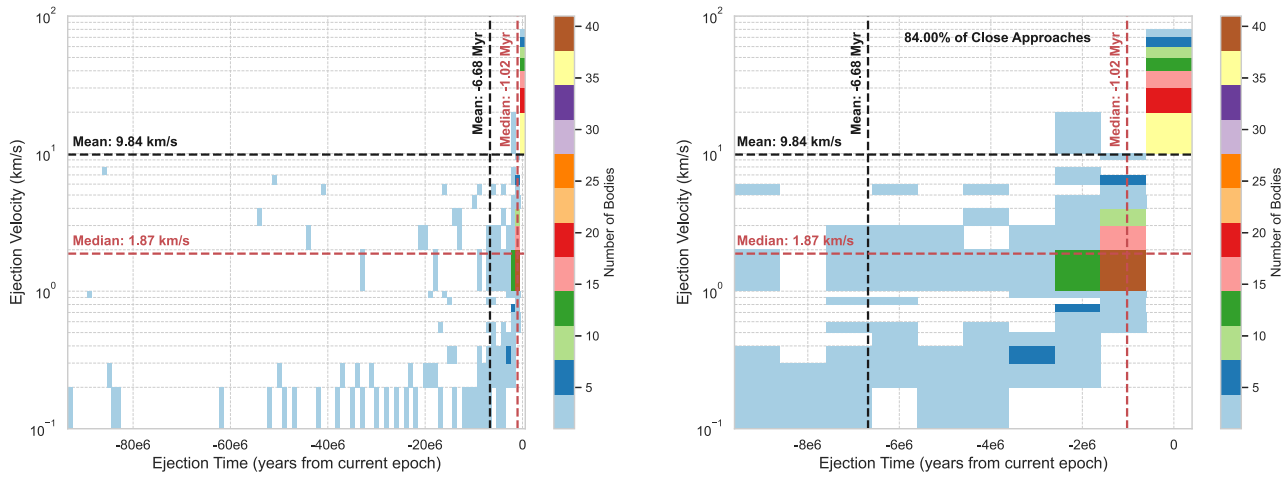


Figure 5. The ejection velocities vs. time of ejection of the α Cen material that enter our Oort cloud. The left figure shows the total distribution while the right zooms into the most common times.

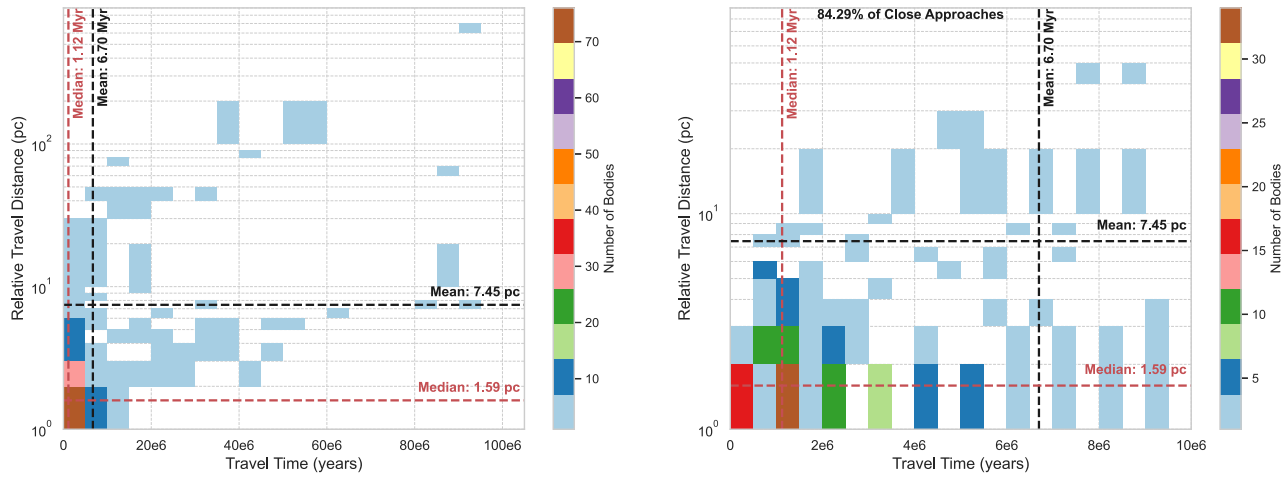


Figure 6. The relative travel distance (the distance a particle travels with respect to α Cen) vs. travel time of the α Cen material that enter our Oort cloud. The left figure shows the total distribution while the right zooms into the most common times.

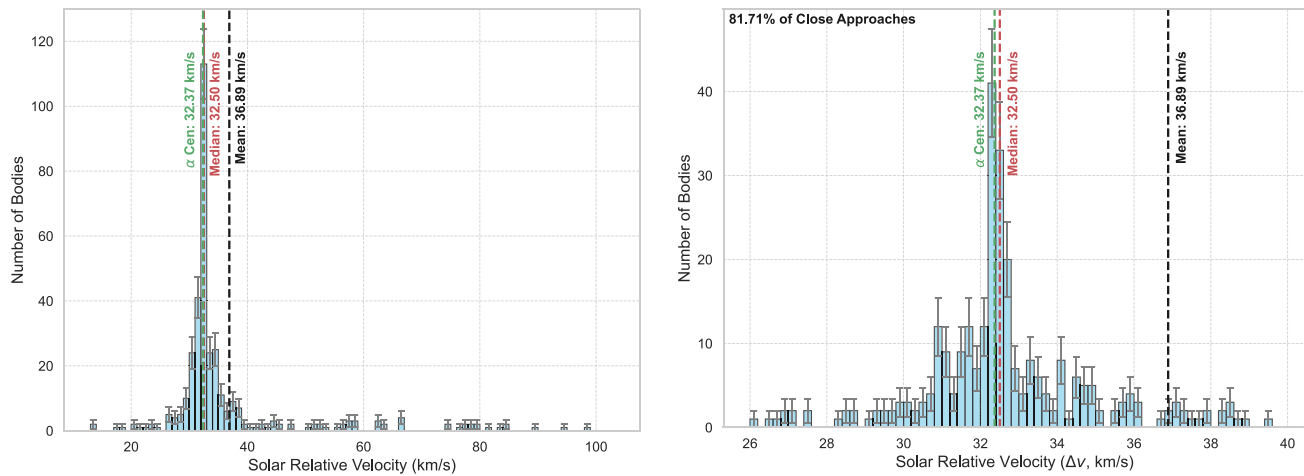


Figure 7. The apparent velocities of the α Cen material that cross our Oort cloud. The left figure shows the total distribution while the right zooms into the most common speeds.

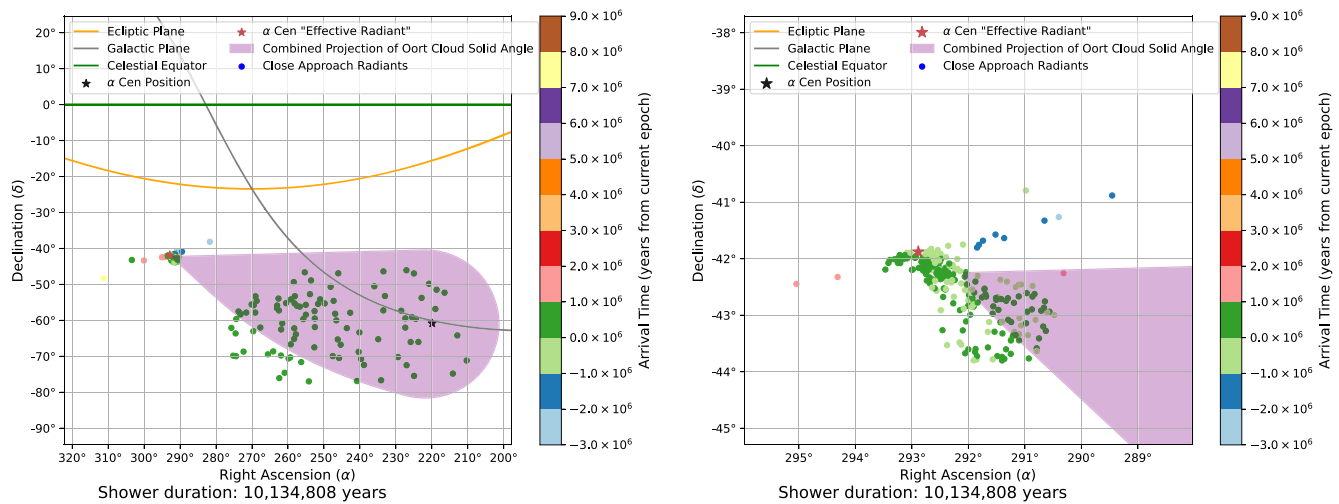


Figure 8. The heliocentric equatorial radiant for the 350 close approaches at the time of their closest solar approach (“Arrival Time”), with the current heliocentric equatorial coordinates of α Cen plotted as a black star, and the “effective radiant” corresponding to α Cen’s apparent velocity is plotted as a red star. The purple shaded region is the combined projection of the effective cross section of the solar system (solid angle size as seen from α Cen), from the start of the simulation up to the current time ($t \approx 0$ yr). The left figure views the entire CA population while the right figure zooms into the region surrounding α Cen’s effective radiant.

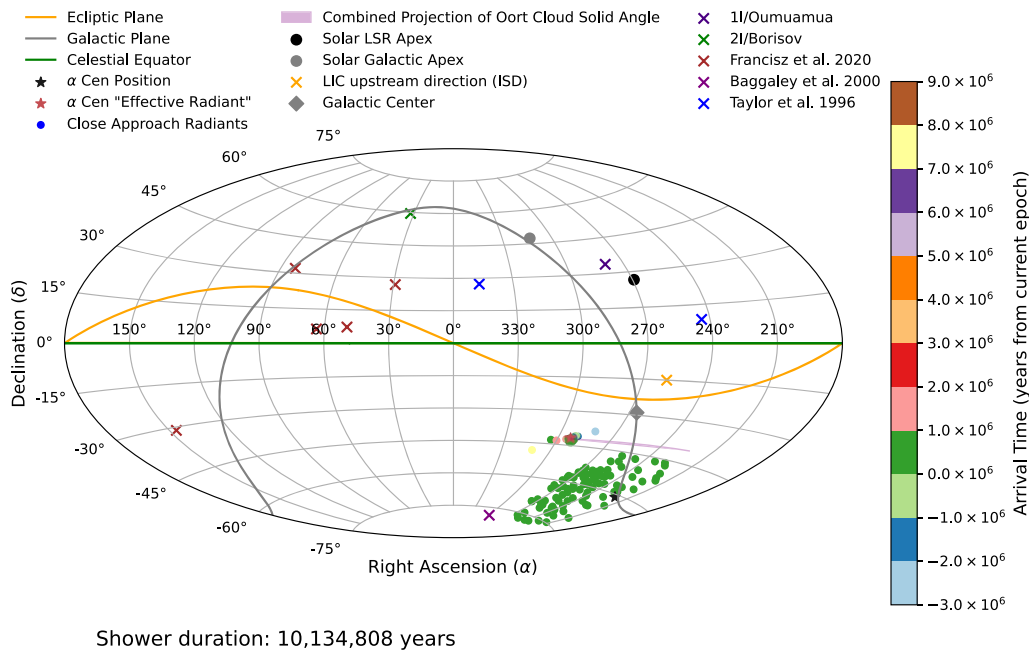


Figure 9. An all-sky version of Figure 8 (see that figure for additional information), with the addition of the two confirmed kilometer-scale interstellar objects (ISOs), five unconfirmed interstellar meteors, three suggested high interstellar meteor flux regions, and the direction of the local interstellar cloud (LIC) upstream direction of interstellar dust (ISD) for comparison (all summarized in Table 2). The solar apex with respect to the local standard of rest (LSR) and within the Milky Way are also included, along with the direction toward the Galactic center. In the full HTML version of this publication, an animation is available showing the radiants of the CAs as they appear during peak intensity, and the progression of α Cen’s position and “effective radiant.” The duration of the animation is 41 s.

(An animation of this figure is available in the [online article](#).)

4. Discussion

Earlier sections have shown that there are plausible dynamical pathways from α Cen to our solar system. We now turn to a discussion of the particle sizes that can survive the passage from α Cen to our solar system, and the expected flux of such particles.

4.1. Grain Sizes and Implications

Small particles traveling through the ISM are subject to a number of effects not modeled here. Thus, although in principle particles may travel between α Cen and our solar

system, whether or not particles—in particular millimeter-sized and smaller particles that might be observed as meteors in Earth’s atmosphere—can survive the journey depends on various factors, such as travel time and speed relative to the ISM. Following N. Murray et al. (2004), we can compute the minimum particle size that can survive the journey from α Cen to our solar system. In particular, they examine three effects: (1) whether the effect of magnetic fields on small charged grains will deflect them significantly, (2) whether drag against the ISM will halt the grains, and (3) whether the grain will be destroyed through sputtering by high-speed gas atoms or by grain–grain collisions.

Table 2
Reported Interstellars, Including LIC Upstream Direction and Significant Directional Values in ICRS Coordinates

Designation	R.A. (α) (deg)	Decl. (δ) (deg)	Category	References
11/Oumuamua	279.6	33.9	ISO	(3)
2I/Borisov	32.6	59.5	ISO	(3)
	29.1	26.8	meteor	(2)
	49.6	7.2	meteor	(2)
	63.7	6.2	meteor	(2)
	82.6	32.0	meteor	(2)
	146.6	-31.1	meteor	(2)
	299.0	-78.4	meteor flux	(1)
	244.0	9.2	meteor flux	(6)
	347.1	27.3	meteor flux	(6)
Local interstellar cloud (LIC) upstream direction	259	8	ISD	(5)
Solar apex relative to local standard of rest	258.7	-15.0		(4)
Solar galactic apex	313.3	47.5		This work
Galactic center—(λ, b)=($0^\circ, 0^\circ$)	266.4	-28.9		(7)

Note. CRS should be defined as International Celestial Reference System.

References. (1) W. J. Baggaley (2000); (2) M. Froncisz et al. (2020); (3) T. Hallatt & P. Wiegert (2020); (4) C. Jaschek & A. Valbousquet (1992); (5) V. J. Sterken et al. (2012); (6) A. D. Taylor et al. (1996); (7) M. J. Reid & A. Brunthaler (2004).

We extracted the relevant parameters for each of the 350 CAs from our simulation and computed the minimum size needed for a grain traveling along that trajectory to survive all three effects (N. Murray et al. 2004’s Equations (44), (45), and (47) relating to drag force, gyroradius, and grain destruction, respectively). We find that minimum particle sizes (a , radius) of $1.05 \leq a \leq 73.22 \mu\text{m}$, with a median of $3.30 \mu\text{m}$, can survive their journey (using values $\rho = 3.5 \text{ g cm}^{-3}$; $n_{\text{H}} = 1 \text{ cm}^{-3}$; $U = 1\text{V}$, $B = 5\mu\text{G}$; and $T_{\text{gas}} = 10^6 \text{ K}$). To clarify, our median particle size corresponds to a simulated particle that traveled 1.5 pc in $\alpha \text{ Cen}$ ’s comoving frame at an average velocity of 16 km s^{-1} with respect to the circular velocity of the Sun. At this size and speed, the particle can travel 125 pc in the ISM before grain destruction becomes relevant, 4200 pc for ISM drag, and only 1.5 pc for magnetic forces, and thus, our typical particles are effectively magnetically limited. In fact, all of our particles are limited by magnetic forces.

At these small grain sizes, detectability by meteor radar instruments is limited. The practical lower limit to the size of meteoroids detected by currently operating meteor patrol radars like the CMOR (described further in the next section) is roughly $100 \mu\text{m}$ in diameter. Particles at these sizes travel unimpeded for large distances across the Galaxy. For example, a $100 \mu\text{m}$ particle traveling at our typical speed of 17 km s^{-1} could travel 369 pc before being substantially deflected by magnetic fields. Only one of our simulated particles traveled farther (600 pc), while the remaining 349 traveled $< 200 \text{ pc}$ (Figure 6). We therefore adopt a fiducial meteor size of $100 \mu\text{m}$ (diameter) at which the effects of drag, grain destruction, and magnetic deflection do not present a concern in this context. But in any case, from this analysis, we can conclude that our results are applicable from submillimeter particles up to large telescopically observable asteroids or comets.

We note an important size-independent effect that we ignore is the effect of encounters with GMCs, which can create $\sim 10 \text{ km s}^{-1}$ kicks in velocity on objects orbiting with the Milky Way’s disk, and which occur with a characteristic time of 200 Myr (R. Wielen 1977; D. Mihalas & J. Binney 1981). Our simulations here only extend for 100 Myr, and most of the

mass transfer observed occurs over much shorter timescales, so the effect of GMCs on our results is likely negligible.

4.2. Mass/Number Influx Estimates

We can now begin to draw some conclusions on how many $\alpha \text{ Cen}$ particles we may expect to see in the solar system currently and during the peak intensity of the shower. To do this, we must estimate the ejection rate for the $\alpha \text{ Cen}$ system.

Unfortunately, the rate of ejection of material from $\alpha \text{ Cen}$ is poorly constrained. As a first-order approximation, we assume that $\alpha \text{ Cen}$ ejects material at a rate similar to that of the solar system at the current time. At macroscopic sizes, this includes the ejection of asteroids recently escaped from the asteroid belt, as well as the ejection of comets arriving from the OC or stripped from it by the Galactic tidal field. The best quantified of these processes is the ejection of new OC comets, and we will adopt it here as a proxy for our total ejection rate. Comets newly arriving in the inner solar system from the OC are on nearly unbound orbits, and planetary perturbations will scatter half onto more tightly bound orbits and eject the other half (P. R. Weissman 1979; P. Wiegert & S. Tremaine 1999). So, the rate at which OC comets are ejected in our solar system is roughly half the arrival rate of new OC comets to the inner solar system. The rates of long-period comet detection have been carefully studied. B. Boe et al. (2019) report a size–frequency distribution (SFD) of long-period comets, which are mostly new OC comets, based on observations from Pan-STARRS. During the 6.8 yr survey in question, 229 comets were observed with a typical nucleus size of 4 km. Extending this to smaller but still telescopically accessible sizes using their observed size distribution, this corresponds to 1.76×10^3 new OC objects of 100 m or greater diameter passing perihelion per year, or an ejection rate of $\sim 0.5 \times 1.76 \times 10^3 = 9 \times 10^2$ objects $>100 \text{ m yr}^{-1}$. Therefore, if $\alpha \text{ Cen}$ ejects cometary material at a rate equal to our own solar system, then 9×10^8 comets are ejected per Myr. In our simulations, 10^4 particles are ejected every Myr, so a single simulated particle represents $f_{\text{sim}} = 9 \times 10^8 / 10^4 = 9 \times 10^4$ real particles $>100 \text{ m}$ in diameter.

In our simulations, at the current time, approximately five particles are seen to enter the OC per 10,000 yr (Figure 4). Since each of our simulated particles corresponds to f_{sim} real objects larger than 100 m, this translates into a flux into the OC of $5f_{\text{sim}}/10^4 = 45$ macroscopic particles per year.

Particles from α Cen arrive with typical speeds of 32 km s^{-1} relative to the Sun and so take an average of $\sim 20,000$ yr to cross the 200,000 au diameter of the OC (assuming an average chord length of $4R/3$). So an arrival flux of N per year into the OC translates into $2 \times 10^4 N = 9 \times 10^5$ macroscopic particles from α Cen currently within the OC. Although possibly abundant within the notional bounds of our solar system, this number decreases significantly if we consider that our practical observation limit is only ≤ 10 au from the Sun. This region is only 10^{-12} the volume of the OC and thus only expected to contain an object from α Cen with the probability $\sim 10^{-6}$.

Telescopically observable α Cen ISOs are thus expected to be rare. But what about smaller particles, which are likely more abundant and could be observed by meteor monitoring systems? Determining the rate of ejection of particles at these sizes is even more difficult. We note here that B. Boe et al. (2019) SFD extends to ~ 120 m: ideally, we would extend this to millimeter-sized particles, but the uncertainty in this process is too large to accurately make any sort of prediction on this basis.

Instead, for the sake of argument, let us consider the observability of an equivalent mass rate of ejection of $100 \mu\text{m}$ particles, about the smallest meteor sizes routinely detected in Earth's atmosphere. This material could come from cometary material released from new α Cen OC comets and then ejected by planetary perturbations much as the larger comets we considered above are, or could result from the breakup of ejected macroscopic comets in space. The question of mass ejection rates at these sizes surely deserves further study but is beyond the scope of this work.

Using our smallest comet size in this range (100 m) and an average comet density of 400 kg m^{-3} (M. F. A'Hearn et al. 2011; H. Sierks et al. 2015), an influx of 45 α Cen bodies 100 m in diameter translates to $\sim 45 \times \frac{4\pi}{3} \times 50^3 \text{ m}^3 \times 400 \text{ kg m}^{-3} \approx 9.4 \times 10^9 \text{ kg}$ of α Cen material per year. This same mass in $100 \mu\text{m}$ diameter particles would provide 10^{18} times more particles (or 4.4×10^{19}). The relative cross section of the Earth to that of the OC is $\left(\frac{6378}{10^5 \times 1.5 \times 10^8} \text{ km}\right)^2 = 1.8 \times 10^{-19}$, and so, we might expect $(4.4 \times 10^{19}) \times (1.8 \times 10^{-19}) \approx 8$ meteors from α Cen to enter the Earth's atmosphere per year as an upper limit. This number is very uncertain by any standard, but reveals that meteors from α Cen may be currently detectable at Earth in small numbers.

During the peak intensity in $\sim 28,000$ yr, we expect these values to increase by a factor of ~ 10 : an influx of $\sim 10^3$ macroscopic particles per year; 10^7 within the OC; a 10^{-5} probability of one being within 10 au of the Sun; and 10^2 Earth intersecting $100 \mu\text{m}$ particles per year.

To place this flux in context, we can compare it to the observed number of solar system meteors that enter our atmosphere at these sizes. The CMOR (A. Webster et al. 2004) is an all-sky meteor patrol radar that observes meteors above southwestern Ontario in Canada 24 hr a day down to a limiting mass of 10^{-8} kg , corresponding to $200 \mu\text{m}$ (diameter) sizes for a density of 1000 kg m^{-3} ([574, 135 μm] for densities of [100, 7800 kg m^{-3}] corresponding to cometary material and iron respectively). CMOR observations provide the best measurements of meteor fluxes at sizes comparable to those we are considering here. M. Froncisz et al. (2020) provide the number

of meteoroid orbits measured by CMOR and an integrated time–area product over 7.5 yr of operation. From this, we can estimate that roughly 7×10^{12} meteoroids of all types (but essentially all from our solar system) enter Earth's atmosphere per year. As a result, only about 1 in 10^{12} $100 \mu\text{m}$ sized meteors observed at Earth might be from α Cen.

Meteors from α Cen are extremely rare events, vastly outnumbered by those originating in our solar system. Nevertheless, understanding the properties of particles that could be arriving from α Cen will aid in the detection of these elusive but potentially highly informative visitors.

5. Conclusions

This work examines the possibility of material from our nearest stellar neighbor α Cen arriving at our solar system. In particular, we explored the delivery of submillimeter- through kilometer-sized bodies ejected from that system by gravitational scattering within the last 100 Myr.

Our study lead us to the following conclusions:

1. Material from α Cen can reach and likely is already within our solar system.
2. Most material arriving from α Cen has traveled for < 10 Myr.
3. Material that reaches us typically left α Cen with low ($v_\infty < 2 \text{ km s}^{-1}$) asymptotic speeds.
4. The delivery of particles from α Cen is concentrated during a ~ 10 Myr period, with the peak intensity centered after α Cen's closest approach ($t \approx 28,000$ yr).
5. The median velocity of the ejecta relative to the Sun at the time of CA is $\Delta v = 32.50 \text{ km s}^{-1}$, similar to the current relative velocity of α Cen ($\Delta v = 32.37 \text{ km s}^{-1}$, M. Wenger et al. 2000).
6. If any of this material enters the inner solar system, its fall into the Sun's gravitational well will accelerate it to a typical heliocentric velocity $v_{\text{hel}} = 53 \text{ km s}^{-1}$ at 1 au.
7. The expected radiant of α Cen meteors at the current time ($(\alpha, \delta) = (292^\circ \pm 1^\circ, -43^\circ \pm 2^\circ)$) largely corresponds to α Cen's effective radiant, set by that system's velocity relative to the Sun. However, as α Cen's closest approach nears, the radiant will move and have a larger spread ($(\alpha, \delta) = (249^\circ \pm 17^\circ, -61^\circ \pm 8^\circ)$) resulting from the increased range of allowable ejection speeds and directions near the closest approach when the solar system's apparent cross section is largest.
8. We expect that particles larger than a few microns in size are able to survive the journey from α Cen.
9. If α Cen ejects comets at a rate comparable to the current solar system rate, we expect $\sim 10^6$ macroscopic α Cen particles to be currently within our solar system, although the chance of one being detectable (that is, within 10 au of our star) is only one in a million.
10. Estimates of α Cen meteor fluxes at the Earth are extremely uncertain, but a first approximation predicts perhaps as many as ~ 10 detectable meteors per year in Earth's atmosphere currently, and that the current rate should increase by a factor of 10 in the next 28,000 yr.

A thorough understanding of the mechanisms by which material could be transferred from α Cen to the solar system not only deepens our knowledge of interstellar transport but also opens new pathways for exploring the interconnectedness of stellar systems and the potential for material exchange across the Galaxy.

Acknowledgments

This work was supported in part by the NASA Meteoroid Environment Office under Cooperative Agreement No. 80NSSC24M0060 and by the Natural Sciences and Engineering Research Council of Canada (NSERC) Discovery Grant program (grant No. RGPIN-2024-05200).

This research has made use of the SIMBAD database, operated at CDS, Strasbourg, France.

The authors thank the anonymous reviewers and the editor for their constructive feedback, which has helped improve this manuscript.

ORCID iDs

Cole R. Gregg  <https://orcid.org/0000-0001-8927-7708>

Paul A. Wiegert  <https://orcid.org/0000-0002-1914-5352>

References

- Adams, F. C. 2010, *ARA&A*, 48, 47
- Adams, F. C., & Napier, K. J. 2022, *AsBio*, 22, 1429
- Akeson, R., Beichman, C., Kervella, P., Fomalont, E., & Benedict, G. F. 2021, *AJ*, 162, 14
- Altobelli, N., Kempf, S., Landgraf, M., et al. 2003, *JGRA*, 108, 8032
- Anglada-Escudé, G., Amado, P. J., Barnes, J., et al. 2016, *Natur*, 536, 437
- A'Hearn, M. F., Belton, M. J., Delamere, W. A., et al. 2011, *Sci*, 332, 1396
- Baggaley, W. J. 2000, *JGR*, 105, 10353
- Baguhl, M., Grün, E., Hamilton, D., et al. 1995, *SSRv*, 72, 471
- Bailer-Jones, C. A. L., Farnocchia, D., Meech, K. J., et al. 2018, *AJ*, 156, 205
- Binney, J., & Tremaine, S. 2008, *Galactic Dynamics* (2nd ed.; Princeton, NJ: Princeton Univ. Press)
- Boe, B., Jedicke, R., Meech, K. J., et al. 2019, *Icar*, 333, 252
- Bovy, J. 2015, *ApJS*, 216, 29
- Brasser, R., & Morbidelli, A. 2013, *Icar*, 225, 40
- Charnoz, S., & Morbidelli, A. 2003, *Icar*, 166, 141
- Chen, B., Stoughton, C., Smith, J. A., et al. 2001, *ApJ*, 553, 184
- Correa-Otto, J. A., & Calandra, M. F. 2019, *MNRAS*, 490, 2495
- Cuello, N., & Sucerquia, M. 2024, *Univ*, 10, 64
- Ćuk, M. 2018, *ApJL*, 852, L15
- Damasso, M., Del Sordo, F., Anglada-Escudé, G., et al. 2020, *SciA*, 6, eaax7467
- Dauphole, B., & Colin, J. 1995, *A&A*, 300, 117
- Dehnen, W., & Hasanuddin 2018, *MNRAS*, 479, 4720
- Duncan, M., Quinn, T., & Tremaine, S. 1987, *AJ*, 94, 1330
- Evans, D. 1967, in *IAU Symp. 030, Determination of Radial Velocities and their Applications*, ed. A. H. Batten & J. F. Heard (Cambridge: Cambridge Univ. Press), 57
- Faria, J. P., Suárez Mascareño, A., Figueira, P., et al. 2022, *A&A*, 658, A115
- Fehlberg, E. 1974, *Classical Seventh-, Sixth-, and Fifth-order Runge–Kutta–Nyström Formulas with Stepsize Control for General Second-order Differential Equations* NASA-TR-R-432, NASA, <https://ntrs.nasa.gov/citations/19740026877>
- Fernandez, J., & Ip, W.-H. 1984, *Icar*, 58, 109
- Francisz, M., Brown, P., & Weryk, R. J. 2020, *P&SS*, 190, 104980
- Gillessen, S., Eisenhauer, F., Trippe, S., et al. 2009, *ApJ*, 692, 1075
- Gratton, R., Zurlo, A., Le Coroller, H., et al. 2020, *A&A*, 638, A120
- Grishin, E., Perets, H. B., & Avni, Y. 2019, *MNRAS*, 487, 3324
- Grün, E., Staubach, P., Baguhl, M., et al. 1997, *Icar*, 129, 270
- Guzik, P., Drahus, M., Rusek, K., et al. 2020, *NatAs*, 4, 53
- Hajdukova, M., Sterken, V., Wiegert, P., & Komoš, L. 2020, *P&SS*, 192, 105060
- Hajduková, M., Stober, G., Barghini, D., et al. 2024, *A&A*, 691, A8
- Hallatt, T., & Wiegert, P. 2020, *AJ*, 159, 147
- Jackson, A. P., Tamayo, D., Hammond, N., Ali-Dib, M., & Rein, H. 2018, *MNRAS*, 478, L49
- Jaschek, C., & Valbousquet, A. 1992, *A&A*, 255, 124
- Joyce, M., & Chaboyer, B. 2018, *ApJ*, 864, 99
- Kervella, P., Thévenin, F., & Lovis, C. 2017, *A&A*, 598, L7
- Meech, K. J., Weryk, R., Micheli, M., et al. 2017, *Natur*, 552, 378
- Mihalas, D., & Binney, J. 1981, *Galactic Astronomy* (New York: Freeman)
- Miyamoto, M., & Nagai, R. 1975, *PASJ*, 27, 533
- Morel, P., Provost, J., Lebreton, Y., Thevenin, F., & Berthomieu, G. 2000, *A&A*, 363, 675
- Moro-Martín, A., & Norman, C. 2022, *ApJ*, 924, 96
- Murray, N., Weingartner, J. C., & Capobianco, C. 2004, *ApJ*, 600, 804
- Osmanov, Z. N. 2024, *The Possibility of Panspermia in the Deep Cosmos by Means of the Planetary Dust Grains*, arXiv:2402.04990
- Portegies Zwart, S. 2021, *A&A*, 647, A136
- Portegies Zwart, S., Torres, S., Pelupessy, I., Bédorf, J., & Cai, M. X. 2018, *MNRAS*, 479, L17
- Rajpaul, V., Aigrain, S., & Roberts, S. J. 2015, *MNRAS: Letters*, 456, L6
- Reid, M. J., & Brunthaler, A. 2004, *ApJ*, 616, 872
- Ribas, I., Gregg, M. D., Boyajian, T. S., & Bolmont, E. 2017, *A&A*, 603, A58
- Safronov, V. S. 1972, in *The Motion, Evolution of Orbits, and Origin of Comets*, ed. G. A. Chebotarev, E. I. Kazimirchak-Polonskaya, & B. G. Marsden (Dordrecht: Springer), 329
- Schönrigh, R., Binney, J., & Dehnen, W. 2010, *MNRAS*, 403, 1829
- Sierks, H., Barbieri, C., Lamy, P. L., et al. 2015, *Sci*, 347, aaa1044
- Smith, H. B., & Sinapayan, L. 2024, *An Agnostic Biosignature Based on Modeling Panspermia and Terraformation*, arxiv:2403.14195
- Smullen, R. A., Kratter, K. M., & Shannon, A. 2016, *MNRAS*, 461, 1288
- Sterken, V. J., Altobelli, N., Kempf, S., et al. 2012, *A&A*, 538, A102
- Taylor, A. D., Baggaley, W. J., & Steel, D. I. 1996, *Natur*, 380, 323
- Thévenin, F., Provost, J., Morel, P., et al. 2002, *A&A*, 392, L9
- Torres, S., Cai, M. X., Brown, A. G. A., & Zwart, S. P. 2019, *A&A*, 629, A139
- Tremaine, S. 1993, in *ASP Conf. Ser. 36, Planets around Pulsars*, ed. J. A. Phillips, S. E. Thorsett, & S. R. Kulkarni (San Francisco, CA: ASP), 335
- Wagner, K., Boehle, A., Pathak, P., et al. 2021, *NatCo*, 12, 922
- Webster, A., Brown, P., Jones, J., Ellis, K., & Campbell-Brown, M. 2004, *ACP*, 4, 679
- Weissman, P. R. 1979, in *IAU Symp. 81, Dynamics of the Solar System*, ed. R. L. Duncombe (Dordrecht: Reidel), 277
- Wenger, M., Ochsenbein, F., Egret, D., et al. 2000, *A&AS*, 143, 9
- Wiegert, P., & Tremaine, S. 1999, *Icar*, 137, 84
- Wielen, R. 1977, *A&A*, 60, 263